



HAL
open science

Reduced graphene oxide decorated with Co₃O₄ nanoparticles (rGO-Co₃O₄) nanocomposite: A reusable catalyst for highly efficient reduction of 4-nitrophenol, and Cr(VI) and dye removal from aqueous solutions

Amer Al-Nafiey, Ahmed Addad, Brigitte Sieber, Guillaume Chastanet, Alexandre Barras, Sabine Szunerits, Rabah Boukherroub

► To cite this version:

Amer Al-Nafiey, Ahmed Addad, Brigitte Sieber, Guillaume Chastanet, Alexandre Barras, et al.. Reduced graphene oxide decorated with Co₃O₄ nanoparticles (rGO-Co₃O₄) nanocomposite: A reusable catalyst for highly efficient reduction of 4-nitrophenol, and Cr(VI) and dye removal from aqueous solutions. *Chemical Engineering Journal*, 2017, 322, pp.375-384. 10.1016/j.cej.2017.04.039 . hal-01520632

HAL Id: hal-01520632

<https://hal.science/hal-01520632>

Submitted on 2 Mar 2021

HAL is a multi-disciplinary open access archive for the deposit and dissemination of scientific research documents, whether they are published or not. The documents may come from teaching and research institutions in France or abroad, or from public or private research centers.

L'archive ouverte pluridisciplinaire **HAL**, est destinée au dépôt et à la diffusion de documents scientifiques de niveau recherche, publiés ou non, émanant des établissements d'enseignement et de recherche français ou étrangers, des laboratoires publics ou privés.

**Reduced graphene oxide decorated with Co₃O₄ nanoparticles (rGO-Co₃O₄)
nanocomposite: A reusable catalyst for highly efficient reduction of 4-
nitrophenol, and Cr(VI) and dye removal from aqueous solutions**

Amer Al Nafiey,^{1,2} Ahmed Addad,² Brigitte Sieber,^{2*} Guillaume Chastanet,³ Alexandre
Barras,¹ Sabine Szunerits,¹ Rabah Boukherroub^{1*}

¹*Univ. Lille, CNRS, Centrale Lille, ISEN, Univ. Valenciennes, UMR 8520 - IEMN, F-59000*

Lille, France

²*Univ. Lille, CNRS, UMR 8207 – UMET, F-59000 Lille, France*

³*Université de Bordeaux, ICMCB, 87 Av. Doc. A. Schweitzer, F-33608 Pessac, France*

*To whom correspondence should be addressed: brigitte.sieber@univ-lille1.fr and rabah.boukherroub@iemn.univ-lille1.fr

Abstract

Water contamination with synthetic dyes and metal ions is an escalating problem, despite the huge research efforts put in the field of water treatment. The paper reports on one-step synthesis of reduced graphene oxide-cobalt oxide nanoparticles (rGO-Co₃O₄) nanocomposite under mild conditions. The nanocomposite material has been characterized using various analytical techniques, including scanning electron microscopy (SEM), energy dispersive X-ray (EDX) spectroscopy, UV-visible spectrophotometry and Fourier-transform infrared (FTIR) spectroscopy. The catalytic properties of the nanocomposite were demonstrated for the sodium borohydride-induced 4-nitrophenol reduction to 4-aminophenol. A full reduction has been achieved within less than 1 min at room temperature. Further, the nanocomposite was successfully applied for Cr(VI) adsorption with a maximum adsorption capacity of 208.8 mg.g⁻¹, which is much higher than that obtained using many other magnetic adsorbents. Finally, the nanocomposite was found to be very efficient for anionic and cationic dye adsorption with complete removal within less than 2 min. The performance of the rGO-Co₃O₄ nanocomposite is quite high as compared to other graphene-based adsorbents. The ferromagnetic properties of the composite allowed effective separation and recyclability of the material by simple application of an external magnet.

Keywords: *Co₃O₄; reduced graphene oxide; 4-nitrophenol; reduction; Cr(VI); dyes; adsorption.*

1. Introduction

With the rapid industrialization, the discharge and release of heavy metal ions and synthetic organic dyes from the textile, paper, and leather industries into the environment represent a serious issue to be addressed since these substances are potentially carcinogenic and mutagenic. To meet environmental regulations and limit the amount of these substances, effluents or water contaminated with these organic and inorganic species must be treated before discharge [1].

Chromium is widely used in industries as for instance, mining, and pigment manufacturing. In aqueous media, Cr exists in two different oxidation states i.e. trivalent Cr(III) and hexavalent Cr(VI) forms. While Cr(III) is less toxic, Cr(VI) is extremely mobile in the environment and carcinogen to living organisms [2]. Due to its bioaccumulation through the food chain, Cr(VI) can cause harm to the human body even at low concentrations. Therefore, it is necessary to reduce the Cr(VI) concentration to a level as low as possible before discharging the industrial waste matter into the environment.

Synthetic dyes represent also an important class of water pollutants. They originate from various sources such as textile, dyeing, printing, paper and pulp, tannery and paint industries. Dyes discharged in water can cause problems to aquatic life and some dyes are even toxic to human life [1]. Most of synthetic dyes are easily dissolved in water in cationic or anionic forms. The cationic dyes include rhodamine B (RhB), methylene blue (MB), methyl violet (MV), malachite green (MG), and the anionic dyes consist of methyl orange (MO) and rose Bengal.

For example, wastewater from textile industries is highly colored by dissolved organic dyes. Color removal from these wastewaters is one of the most difficult tasks, because synthetic dyes and pigments are resistant to biodegradation, and thus remain for a long period of time in the environment. Therefore, from an environmental point of view, the disposal and treatment of organic dyes are of great concern as well as the development of cost-effective methods to remove colored substances from wastewater [1].

To provide solutions for the above-mentioned environmental problems, various approaches and technologies to remove Cr(VI) and synthetic dyes have been described in the literature. These strategies include adsorption, photocatalysis, electro-chemical precipitation, reverse osmosis, and ion exchange [1, 3-6]. Among these methods, only adsorption is a fast, highly efficient, inexpensive, and a widely applicable technique with no discharge of harmful substances.

Even though, adsorption represents an appealing method for environmental remediation, the lack of full recovery of the adsorbent from wastewater may cause a secondary pollution. For that, a magnetic adsorbent is highly desirable, because it allows removal of toxic pollutants (metal ions, dyes) and the adsorbent itself can be recovered easily from water through application of an external magnet.

Despite its short development history, graphene-metal oxide nanocomposites have attracted increasing attention for their applications in environmental and energy-related areas, and GO/rGO-based composites have been successfully applied to treat different types of organic dyes and heavy metal ions [3]. As discussed above, organic dyes exist in ionic (anionic or cationic) forms in water, while GO/rGO are negatively charged, so dye adsorption on GO/rGO is believed to be dominated by electrostatic interactions (anionic-cationic). However, other interactions such as H-bonding and π - π stacking are not excluded during adsorption processes of organic dyes on GO/rGO-based composites [3]. On the one hand, negatively charged graphene oxide (GO) possesses various oxygen containing groups such as OH and COOH groups. As a consequence, it exhibits high adsorption capacity for basic compounds and metal cations. Reduced graphene oxide (rGO), on the other hand, displays a hydrophobic surface and this presents high adsorption capacity for dyes through strong π - π stacking and hydrophobic interactions [3].

An enhanced adsorption ability can be obtained by a modification of GO or rGO with metal oxides or organics. Recent reports have shown that GO/rGO-based composites have an excellent adsorption ability for Cr(VI) [7, 8] and of dyes (methyl orange, methylene blue, rhodamine B) and as such they represent promising adsorbents for water purification [3, 9].

For instance, cobalt oxide Co_3O_4 is a magnetic *p*-type semiconductor with a cubic spinel crystal structure in which Co^{II} and Co^{III} atoms occupy the tetrahedral sites and octahedral sites, respectively [10]. It is a transition metal oxide with interesting optical, electronic, electrochemical, catalytic and electrocatalytic properties [11]. However, the Co_3O_4 outstanding properties are decreased or even lost, because severe particle aggregation takes place during their processing. To limit Co_3O_4 aggregation, their hybridization with carbon-based supports seems to be a very effective approach. For instance, the integration of Co_3O_4 onto graphene matrices endows the resulting materials with enhanced performance [12]. This has also been demonstrated in a few examples for environmental remediation. Co_3O_4 /graphene have been successfully applied for heterogeneous activation of peroxymonosulfate (oxone) for the degradation of Orange II [13-16], phenol [17] by advanced oxidation technology.

To the best of our knowledge, the utilization of rGO- Co_3O_4 nanocomposite for synthetic dyes and metal ions adsorption has been investigated only in a few reports [18]. Indeed, Yavuz *et al.* successfully applied Co_3O_4 /graphene as an effective adsorbent for the retention/separation of Pb(II), Cu(II) and Fe(III) ions from environmental water [18]. In this paper, we took benefit of the high surface area and of the magnetic properties of rGO- Co_3O_4 nanocomposite to improve the catalytic and environmental efficiencies of the process. rGO- Co_3O_4 nanocomposites was used for two environmental applications: Cr(VI) and organic dyes removal from aqueous solution. The description of these applications is preceded with the catalytic reduction 4-nitrophenol to 4-aminophneol by rGO- Co_3O_4 nanocomposite using

sodium borohydride (NaBH_4); this model reaction is commonly used to evaluate the catalytic performance of metal or metal oxide nanoparticles.

2. Experimental

2.1. Preparation of graphene oxide (GO)

GO was synthesized from natural graphite powder according to [19]. A homogeneous GO suspension (0.5 mg/mL) in water was achieved by ultrasonication for 3 h.

2.2. Preparation of reduced graphene oxide/ Co_3O_4 nanocomposite

Different routes have been developed for the synthesis of rGO- Co_3O_4 nanocomposites. Generally, they all require a two-step synthesis with the use of hazard agents and high temperatures (80-600°C) to reduce graphene oxide and anchor cobalt oxide NPs. In the present study, the rGO- Co_3O_4 nanocomposite was synthesized using a one-step, low-cost and simple preparation method based on simultaneous reduction of GO and CoCl_2 using borohydride NaBH_4 as reducing agent at room temperature [20].

rGO- Co_3O_4 nanocomposite was prepared by simultaneous chemical reduction of GO and CoCl_2 with sodium borohydride (NaBH_4). Typically, to 5 mL of 1 mg/mL GO suspension in Milli-Q water, was added 50 mg of CoCl_2 . The resulting mixture was sonicated for 10 min. Then 5 mL of 0.1 M sodium borohydride aqueous solution was added to the mixture at room temperature. A black precipitate was formed spontaneously, which was separated by centrifugation and washed repeatedly with water [20].

2.3. Reduction of 4-nitrophenol to 4-aminophenol catalyzed by rGO- Co_3O_4

The reduction of 4-nitrophenol (4-NP) to 4-aminophenol was carried out at room temperature under stirring. To 3 mL of freshly prepared 0.1 mM 4-nitrophenol aqueous solution was added 300 μL of 0.1 M NaBH_4 and 200 μL of 0.1 mg/mL rGO- Co_3O_4 in water. Following NaBH_4 addition, the solution turned yellow green due to the formation of 4-nitrophenolate. This is

accompanied by a change of the maximum absorption from 317 nm (4-nitrophenol) to 400 nm (4-nitrophenolate). The progress of 4-nitrophenolate reduction to 4-aminophenol catalyzed by rGO-Co₃O₄ was monitored by the decrease of the absorption band at 400 nm using UV-vis spectrophotometry.

2.4. Adsorption studies

The batch adsorption mode was used to study Cr₂O₇²⁻ and dyes adsorption. A stock potassium dichromate (K₂Cr₂O₇) aqueous solution (500 mg/mL) was prepared. Aqueous solutions of different Cr concentrations (25, 50, 100, 200, 300 and 400 mg/L) were prepared by dilution of the stock solution with Milli-Q water. The pH of the Cr solutions was adjusted to 3 with 0.1 M HCl aqueous solution.

The removal ability of rGO-Co₃O₄ nanocomposite of organic dyes in aqueous solutions was investigated for three different dyes (rhodamine B, methyl orange and rose Bengal) at three different concentrations for each dye. For the adsorption experiments, 2 mg of rGO-Co₃O₄ nanocomposite was added to 2 mL of an aqueous solution of rhodamine B (RhB), methyl orange (MO) or rose Bengal (RB) (5, 10 or 15 μM) at room temperature at pH 7.

The % of removal of Cr(VI) and dyes is calculated using:

$$\text{Removal (\%)} = (C_0 - C_f) / C_0 \times 100$$

where C₀ is the initial concentration and C_f the final concentration of Cr(VI) ions or dyes.

3. Results and discussion

3.1. Characterization of rGO-Co₃O₄ nanocomposite

The morphology and microstructures of the as-synthesized samples were investigated by FE-SEM (**Fig. 1**). **Figure 1a** displays the SEM image of the initial GO, consisting of crumpled sheets. Similarly, the SEM image of the as-synthesized rGO-Co₃O₄ nanocomposite comprises

aggregated and crumpled sheets of many graphene sheets along with Co_3O_4 nanoparticles (**Fig. 1b**).

The TEM image of the prepared rGO- Co_3O_4 nanocomposite displays Co_3O_4 NPs of 2-10 nm in size distributed on the rGO sheets (**Fig. 1c**). Additionally, the HR-TEM image of a single Co_3O_4 NP exhibits an interplanar distance between adjacent planes of 0.47 nm, corresponding to the interplanar spacing of (111) plane of Co_3O_4 (Inset **Fig. 1c**) [20]. The diffraction rings of the selected-area electron diffraction (SAED) pattern consists of five diffraction rings corresponding to the (220), (311), (400), (440), and (511) planes of Co_3O_4 (**Fig. 1d**).

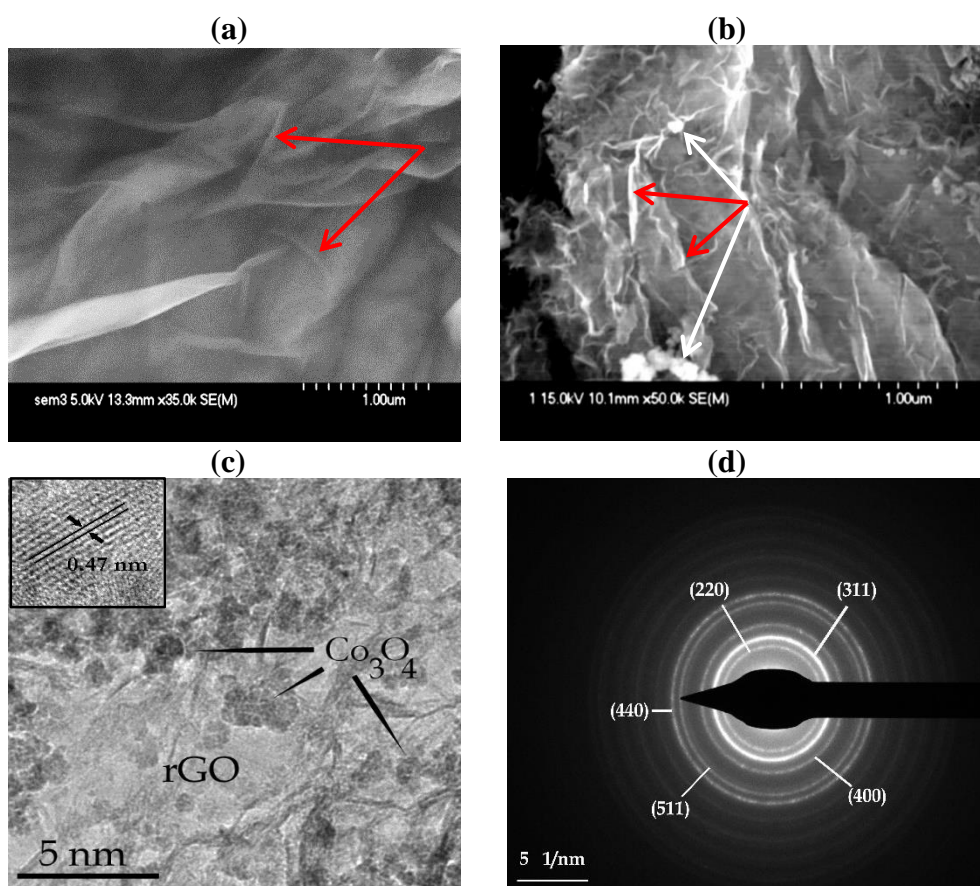


Figure 1. FE-SEM images of the (a) GO and (b) rGO- Co_3O_4 nanocomposite. Red arrows point toward the folds which connect the different GO/rGO sheets. The white arrows point toward Co_3O_4 nanoparticles; (c) TEM image of Co_3O_4 nanoparticles on rGO sheet. The inset is a HR-TEM image of a nanoparticle, (d) SAED of rGO/ Co_3O_4 .

The as-synthesized rGO-Co₃O₄ nanocomposite contains only cobalt, carbon, and oxygen, as revealed by TEM-EDX analysis (**Fig. S1**), consistent with the chemical composition of the material. Some of the carbon signal may originate from the carbon grid onto which the sample was deposited for TEM and EDX analysis.

The cobalt content in the synthesized rGO-Co₃O₄ nanocomposite was estimated by ICP-AES analysis, and the results showed a Co loading of 50.4 g in 100 g of composite.

Figure 2 depicts the UV-vis absorption spectra of GO, rGO and rGO-Co₃O₄ nanocomposite. The UV-vis absorption spectrum of GO displays characteristic absorption peaks at 225 nm and a shoulder at around 300 nm due to π - π^* of aromatic carbon bonds and n - π^* transition of C=O bonds, respectively (**Fig.2**, red trace). Upon GO reduction with NaBH₄ at room temperature, a red shift of the GO absorption band to 260 nm is observed, suggesting partial restoration of the aromatic network (**Fig.2**, blue trace).

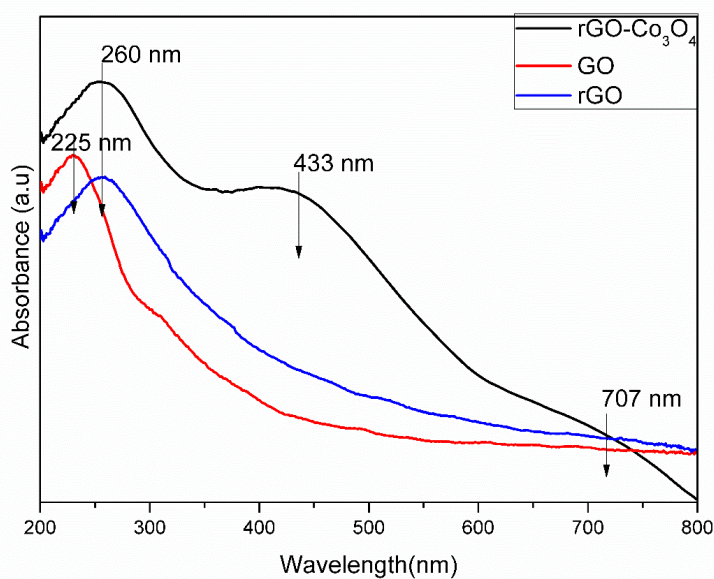


Figure 2. UV-visible absorption spectra of GO before (red), rGO (blue) and rGO-Co₃O₄ nanocomposite (black).

NaBH₄ reduction of a mixture of GO and CoCl₂ aqueous solution induces also a red-shift of the absorption band of GO from 225 to 260 nm as well as the appearance of a new strong band

at 433 nm due to Co_3O_4 NPs (**Fig. 2**, black trace) [21, 22]. The results suggest that GO nanosheets have been reduced to rGO and the sp^2 network within the GO nanosheets was partially restored upon reaction with cobalt chloride and NaBH_4 . The presence of a new band at 433 nm evidences that the cobalt oxide nanoparticles have been anchored onto the rGO sheets, suggesting a strong interaction between rGO and Co_3O_4 NPs. Co_3O_4 NPs are 2-5 nm in size as evaluated by X-ray diffraction (XRD) and transmission electron microscopy (TEM) analysis [20].

The FTIR spectra show remarkable differences between GO and rGO- Co_3O_4 (**Fig. 3**). For GO, a strong and broad absorption ascribed to O–H vibration mode, and the C=O stretching mode of COOH groups situated at the edges of GO sheets are observed at 3404 and 1740 cm^{-1} , respectively.

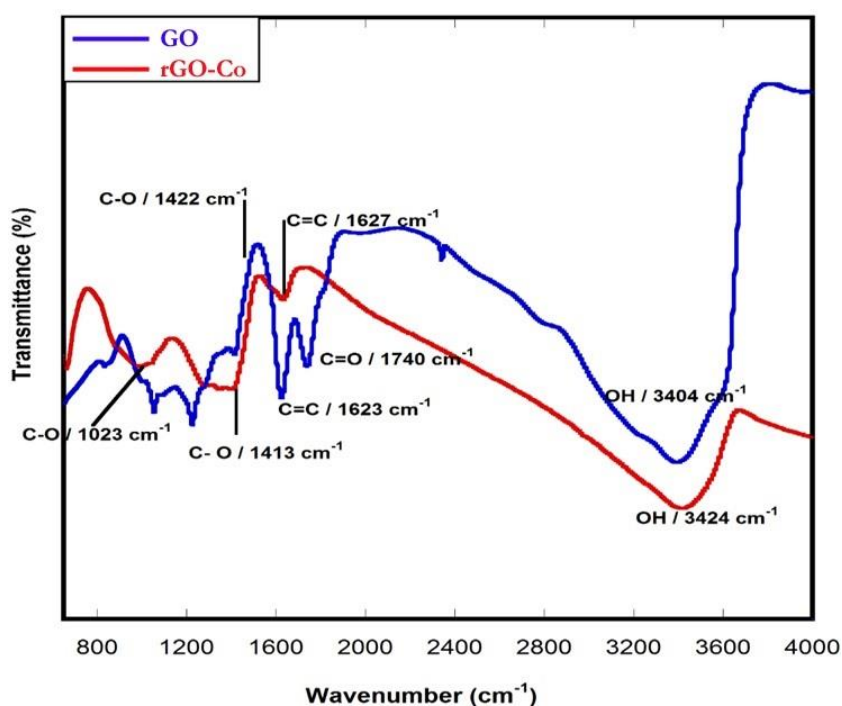


Figure 3: Infrared spectra of GO (blue) and rGO- Co_3O_4 nanocomposite (red).

The vibration mode at 1422 cm^{-1} may be due to bending vibrations of tertiary C–OH groups or to bending vibration of C–H bonds. But, due to the presence of OH groups on rGO- Co_3O_4 composites (**Fig. 3**) and to the usual existence of hydroxyls and carboxyl group on rGO, we

suggest that the 1422 cm^{-1} vibration modes are more likely due to C–OH groups. The band at 1023 cm^{-1} is attributed to stretching vibrations of C–O groups, while the band at 1623 cm^{-1} is attributed to C=C stretching vibration as part of the ring breathing mode in the GO skeleton [23]. By contrast, for the rGO-Co₃O₄ nanocomposite, the O–H absorption band is shifted to 3424 cm^{-1} , while the skeletal vibration band C=C at 1623 cm^{-1} is shifted to 1627 cm^{-1} . Moreover, the stretching band of C=O at 1740 cm^{-1} disappears, suggesting that GO was reduced to rGO during the chemical process [24].

The rGO-Co₃O₄ NPs hybrid exhibits typical ferromagnetic behavior with a saturation magnetization (M_s) of $0.1\text{ emu}\cdot\text{g}^{-1}$ and a hysteresis of 115 Oe at 300 K (27°C), as shown by the magnetic hysteresis loop in **Fig. 4a**.

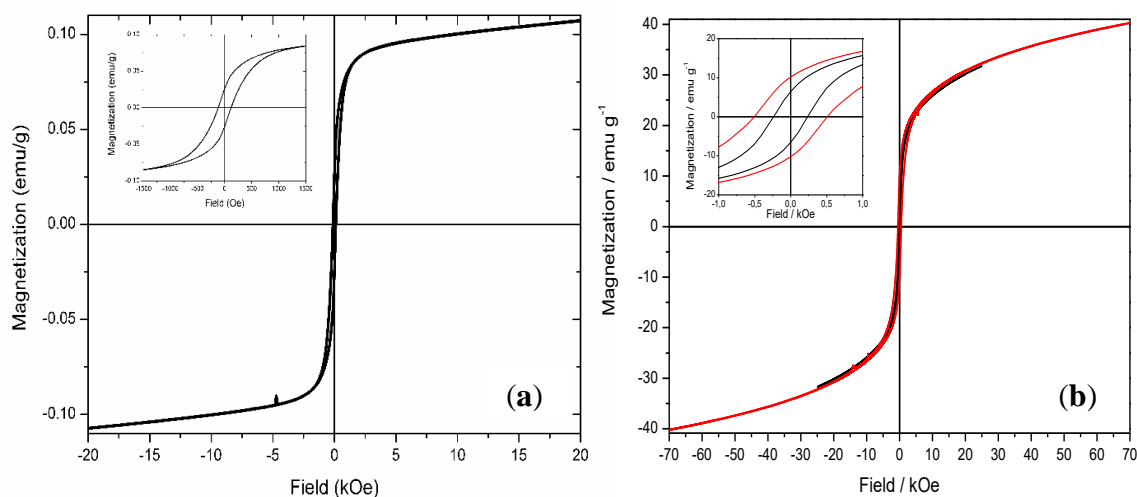


Figure 4. Magnetic hysteresis loops of rGO-Co₃O₄ nanocomposite at a) 300 K and b) 2K (red) and 4K (dark).

The coercive force increases as the temperature is decreasing, to 495 Oe at 2 K; similarly, the saturation magnetization (M_s) increased to $40\text{ emu}\cdot\text{g}^{-1}$ (**Fig. 4b**). This value can facilitate the recycling of the nanocomposite catalyst by a low energy-saving magnetic separation process.

3.2. Applications

3.2.1. Catalytic reduction of 4-nitrophenol

The catalytic activity of the rGO-Co₃O₄ nanocomposite was evaluated for 4-nitrophenol (4-NP) reduction to 4-aminophenol (4-AP) in the presence of excess NaBH₄. This model reaction is commonly used in catalytic processes to examine the catalytic performance of metal or metal oxide nanoparticles (**Fig. 5**).

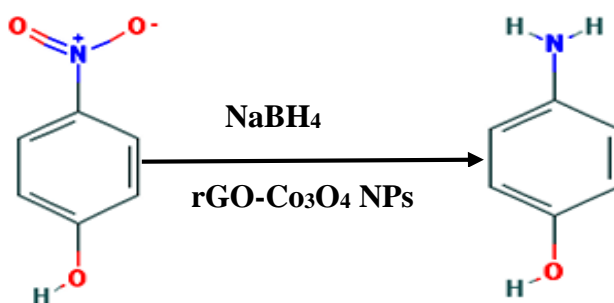


Figure 5: Schematic illustration of 4-nitrophenol reduction by NaBH₄ catalyzed by rGO-Co₃O₄ nanocomposite.

Typically, two aqueous solutions of 0.1 mM of 4-NP and 0.1 M NaBH₄ were prepared. Then a mixture of 3 mL of 4-NP and 0.5 mL of NaBH₄ was prepared from these solutions. During this process, the color changed from transparent to yellow, because 4-nitrophenol was converted to 4-nitrophenolate anion by NaBH₄ (**Figs. 5 and 6**). To this mixture, 100 μL of rGO-Co₃O₄ nanocomposite (0.5 mg mL⁻¹) catalyst was added at room temperature; the yellow-green color disappeared (**Fig. 6**).



Figure 6: Images illustrating the catalytic reduction of 4-NP to 4-AP using rGO-Co₃O₄ nanocomposite as catalyst and its separation at the end of the process using an external magnet.

The progress of the reduction reaction was monitored by UV-vis spectroscopy (**Fig. 7**). The UV-vis absorption spectrum of 4-NP exhibits an absorbance peak at 317 nm (**Fig. 7**, black curve). Upon addition of NaBH₄, the absorption maximum shifts to 400 nm accompanied by a color change from transparent to light yellow due to the formation of p-nitrophenolate ion (**Fig. 7**, red curve). In absence of rGO-Co₃O₄ NPs catalyst, the peak due to 4-nitrophenolate ion at 400 nm is stable and remains unaltered even after two days, confirming the catalytic activity of the nanocomposite. Thus, the catalytic reduction of 4-NP to 4-AP can be monitored by following the decay of the characteristic absorption peak of 4-nitrophenoxide at 400 nm [25].

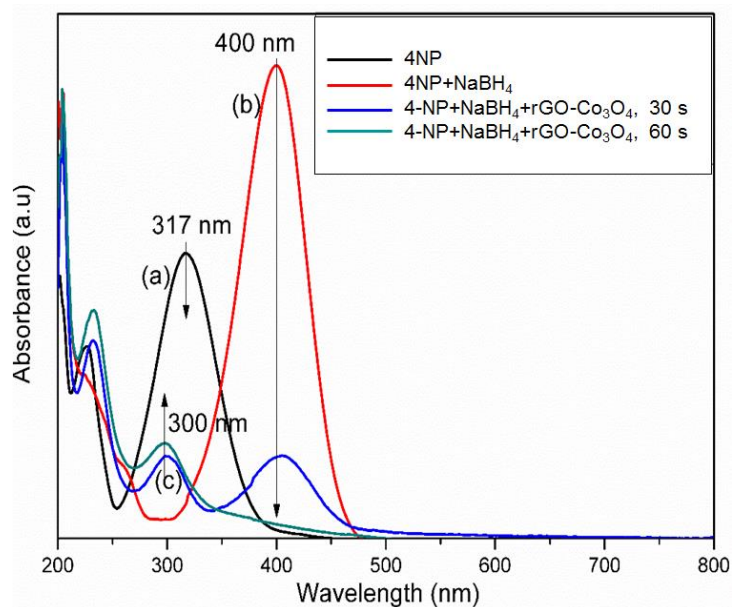


Figure 7: UV–visible spectra of 4-NP (a), 4-NP before (b) and after (c) addition of 100 μL of $\text{rGO-Co}_3\text{O}_4$ nanocomposite (0.5 mg/mL).

The intensity of the 4-nitrophenoxide at 400 nm gradually decreases as the reaction proceeds, indicating the reduction of the $-\text{NO}_2$ group of 4-NP to $-\text{NH}_2$ group (**Fig. 7**, blue curve), and finally disappears after 1 min. Meanwhile, a new peak appears at 300 nm which increases overtime, revealing the reduction of 4-NP to 4-aminophenol (4-AP) successfully catalyzed by the $\text{rGO-Co}_3\text{O}_4$ nanocomposite.

The recyclability of catalysts is an important aspect for a more economical process. Thus recycling catalysis experiments were conducted for the $\text{rGO-Co}_3\text{O}_4$ nanocomposite (0.5 mg/mL) catalyzed the reduction of 4-NP (0.1 mM) with NaBH_4 (0.1 M). At the end of the reaction, the $\text{rGO-Co}_3\text{O}_4$ catalyst was easily recovered from the reaction medium using an external magnet (1 Tesla) (**Fig. 6**), and the supernatant was analyzed using UV-vis spectrophotometry. The same procedure was repeated at least ten times in order to explore the reusability and activity of the nanocatalyst. The performance of the as-synthesized $\text{rGO-Co}_3\text{O}_4$ catalyst in repeated cycles of reaction is exhibited in **Fig. S2**. It reveals that the $\text{rGO-Co}_3\text{O}_4$ catalyst has a good stability and activity since it maintains a high performance for ten cycles.

We can consider that the decrease of the reduction time of 4-NP to 4-AP catalyzed by rGO-Co₃O₄ nanocomposite is attributable to the following factor: rGO sheets have high adsorption capacity for 4-NP *via* π - π stacking interactions. As a consequence, high concentration of 4-NP is present near the Co₃O₄ nanoparticles on rGO, leading to better contact between them; the electron transfer from rGO to Co₃O₄ nanoparticles increases the local electron density, improving the uptake of electrons by 4-NP molecules.

3.2.2. Cr(VI) removal from aqueous solution by rGO-Co₃O₄ nanocomposite

3.2.2.1. Adsorption experiments

Cr(VI) aqueous solutions of different Cr concentrations (0.5-300 mg/L) were prepared through successive dilutions of a stock K₂Cr₂O₇ solution (500 mg/mL) with Milli-Q water. The pH value of the Cr solutions was adjusted to 3 with 0.1 M HCl aqueous solution. After the adsorption process, rGO-Co₃O₄ composite was conveniently recovered by magnetic separation, as shown in **Fig. 8**.



Figure 8: Images of Cr(VI) adsorption by rGO-Co₃O₄ nanocomposite and magnetic recovery of the catalyst by application of an external magnet (1 Tesla).

The photographs clearly indicate, that after adsorption of Cr(VI) ions, the yellow color of the metal ion solution is completely lost, which suggests an almost total removal of chromium ions by the rGO-Co₃O₄.

Fig. 9 shows the UV-vis spectrum in the range of 200-500 nm of a Cr(VI) aqueous solution at a concentration of 50 mg/L.

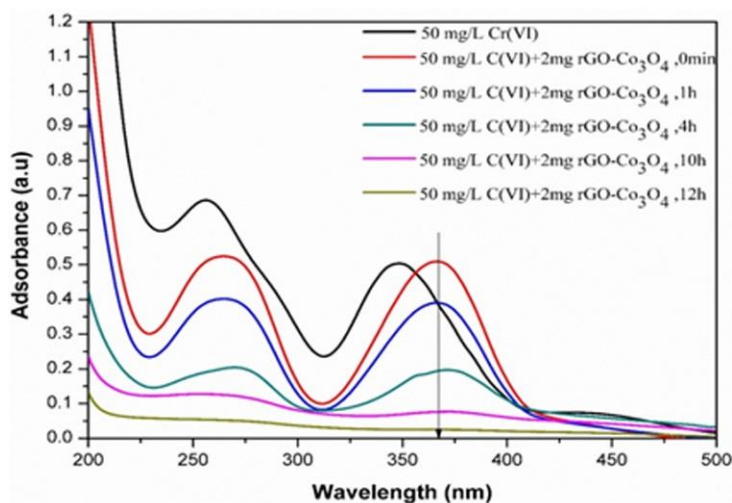


Figure 9: UV–visible absorption spectral evolution with time during adsorption of Cr(VI) ions by rGO-Co₃O₄; Cr (VI) ion concentration: 50 mg/L, adsorbent dosage: 1 mg/mL, temperature: 25°C, pH: 3.0.

It is clearly seen that in the presence of rGO-Co₃O₄ the absorption band of Cr₂O₇²⁻ at 348 nm shifts to 367 nm. This new peak decreases and disappears within 12 h. Also, as noted previously, the color of the solution changes from deep yellow to colorless, confirming the complete adsorption of Cr(VI) by rGO-Co₃O₄.

To check the influence of Cr(VI) concentration in solution on the removal efficiency, the as-synthesized rGO-Co₃O₄ composite (2 mg) was dispersed in 2 mL of Cr(VI) solution at various Cr(VI) concentrations (pH=3) using a shaking speed of 400 rpm for 12 h. The solution was extracted by using a magnet to separate the rGO-Co₃O₄ and the supernatant was analyzed by UV-Vis spectrophotometry in order to determine the residual concentration of Cr(VI). A

linear relationship between the Cr(VI) concentration and the absorbance at 367 nm was established (**Fig. S3**).

3.2.2.2. Adsorption isotherm

The Langmuir model was used to simulate adsorption isotherm of Cr(VI). If the adsorbent exhibits an ideal homogeneous adsorption surface with all the adsorption sites having the same sorption energy independent of surface coverage, the Langmuir model applies. The Cr(VI) removal capacity is thus calculated using:

$$Q = (C_0 - C_e) V/W$$

where Q (mg/g) is the adsorption capacity, C_0 (mg/L) the initial concentration of Cr(VI) ions, C_e (mg/L) the equilibrium concentration of Cr(VI) ions, V (L) the initial volume of Cr(VI) solution, W (g) the mass of the as-prepared rGO-Co₃O₄.

The removal amount of Cr(VI) ions was deduced from a calibration curve obtained from UV-vis absorption measurements from Cr(VI) (0.5-300 mg/L) solutions, as shown in **Fig. S4**.

From the results in **Fig. 10**, it is clear that Cr(VI) ions are favorably adsorbed on the rGO-Co₃O₄ with a maximum adsorption capacity of 208.8 mg.g⁻¹, which is much higher than that obtained using many other magnetic adsorbents such as Fe₃O₄@mTiO₂@GO (118 mg.g⁻¹), graphene oxide decorated with magnetic cyclodextrin (MCGN, 120.0 g.g⁻¹), graphene oxide functionalized with magnetic cyclodextrin-chitosan (CCGO, 67.66 mg.g⁻¹) and iron nanoparticle decorated graphene (G-nZVI, 162.0 mg.g⁻¹), **Table 1**.

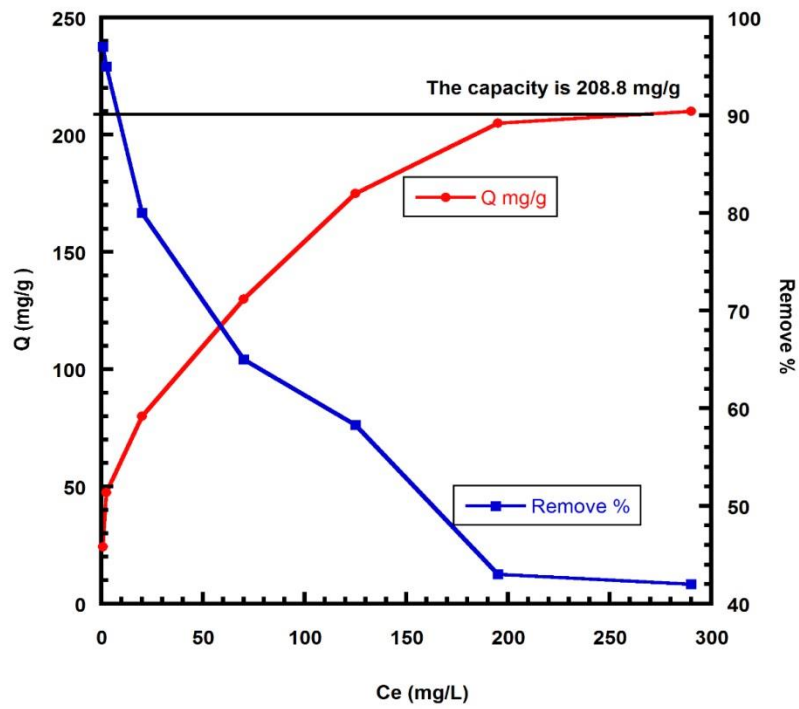


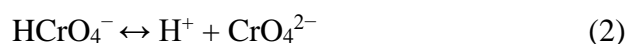
Figure 10: Cr(VI) adsorption isotherms on the rGO-Co₃O₄ at pH 3.0 (Cr(VI) concentration: 0.5-300 mg/L, rGO-Co₃O₄ dosage: 1 mg/mL, pH 3.0, temperature: 25°C, contact time: 12 h).

Adsorbent	Adsorbate	Adsorption capacity (mg.g ⁻¹)	Condition	Ref.
2,6-Diamino pyridine-RGO	Cr(VI)	393.7	C ₀ = 500 mg L ⁻¹	[26]
PPY-GO	Cr(VI)	497.1	pH = 3.0	[27]
PANI-GO	Cr(VI)	1149.4	pH = 3.0; T 298 K	[28]
PPY/Fe ₃ O ₄	Cr(VI)	243.9	pH = 2.0; T 298 K	[29]
Ni-rGO	Cr(VI)	≥98%, 4 min Cr = 0.37 mM	pH = 2.0; T 298 K	[30]
PEI-GO	Cr(VI)	539.53	pH = 2.0; T 298 K	[31]
Fe ₃ O ₄ @mTiO ₂ @GO	Cr(VI)	117.94	pH = 2.0; T 303 K	[32]
Graphene sand composite	Cr(VI)	2859.38	pH = 1.5; T 298 K	[33]
MCGN	Cr(VI)	120.0	pH = 3; T 298 K	[34]
CCGO	Cr(VI)	67.66	pH = 3; T 298 K	[35]
G-nZVI ZVI (zero valent iron)	Cr(VI)	162.0	pH = 3; T 323 K	[36]

Table 1. Adsorption capacity of Cr(VI) from wastewater using different adsorbents.

The pH of the solution is known to be one of the most important parameters affecting the adsorption characteristics of ionic adsorbates. The relation between Cr(VI) adsorption capacity and initial pH of solution is depicted in **Fig. S5**. The higher adsorption capacity observed at a lower solution pH could be explained by the higher surface charge of the adsorbent, but also

by the degree of ionization of the adsorbate. Chromium occurs in different anionic forms in aqueous solution (*i.e.*, $\text{H}_2\text{Cr}_2\text{O}_7$, $\text{Cr}_2\text{O}_7^{2-}$, HCrO_4^- , CrO_4^{2-} and HCr_2O_7^-), depending on the solution pH and concentration [33]. The following equilibria exist in an aqueous solution (1-3):



The results in **Fig. S5** clearly reveal that the maximum adsorption of Cr(VI) is achieved in acidic media. This may be due to the fact that in the aqueous solution several forms of Cr(VI) ions exist such as $\text{Cr}_2\text{O}_7^{2-}$ and hydrogen chromate (HCrO_4^-), which are the dominant species in acidic media. In this case, the negatively charged HCrO_4^- can be adsorbed on the rGO- Co_3O_4 through electrostatic interaction. In acidic medium, high concentration of H^+ ions is present which are able to neutralize the negatively charged adsorbent surface, thereby enhancing dichromate ions diffusion at low pH [37]. In alkaline media, surface protonation decreases gradually and only chromate (CrO_4^{2-}) ions remain as stable species. Therefore, when the solution pH is changed, the adsorption capacity of the rGO- Co_3O_4 for Cr(VI) is dominated by the existing form of Cr(VI) ions in solution.

To gain a better understanding on the adsorption mechanism, we have measured the zeta potential of rGO- Co_3O_4 in water (**Fig. S6**). A zeta potential of 17.0 ± 1.5 mV was recorded. According to Eqs (1-3), Cr(VI) exists mostly in its anionic form in acidic pH, suggesting that electrostatic interactions are dominant for Cr(VI) adsorption on rGO- Co_3O_4 although one cannot exclude Cr(VI) interaction with the oxygen-containing groups on the nanocomposite surface.

We have used the Langmuir isotherm to describe the equilibrium established between adsorbed Cr(VI) ions on the rGO-CO₃O₄ adsorbent (Q_e) and Cr(VI) ions remaining in solution (C_e) at a constant temperature. Adsorption isotherms of the type Q_e vs C_e was used to verify the isotherm model. The equilibrium adsorption isotherm was fitted with the Langmuir model using the following equation:

$$Q_e = \frac{Q_{max} b C_e}{1 + b C_e} \quad \text{or} \quad \frac{C_e}{Q_e} = \frac{1}{Q_{max} b} + \frac{C_e}{Q_{max}}$$

where C_e (mg/L) is the equilibrium concentration of Cr (VI) ions, Q_e (mg/g) the amount of adsorbed Cr(IV) ions, Q_{max} (mg/g) the maximum adsorption capacity, and b (L/mg) the Langmuir isotherm coefficient.

The Langmuir isotherm parameters are obtained from the linear fit shown in **Fig. S7**. The Langmuir isotherm model gives a maximum adsorption capacity of 222.22 mg.g⁻¹ for Cr(VI), which is very close to the experimental value of 208.8 mg.g⁻¹.

3.2.3. Dye removal from aqueous solution by rGO-CO₃O₄ nanocomposite

The removal ability of rGO-CO₃O₄ nanocomposite of organic dyes in aqueous solution has been investigated for three different dyes (one cationic dye, Rhodamine B and two anionic dyes, Methyl Orange and Rose Bengal) at three different concentrations for each dye. For the adsorption experiments, 2 mg of rGO-CO₃O₄ composite was added to 2 mL of an aqueous solution of RhB, MO or RB (5, 10 or 15 μM) at room temperature and pH 7.

Dye removal efficiency was calculated by recording the dye concentration before and after adsorption using UV-vis spectrophotometry.

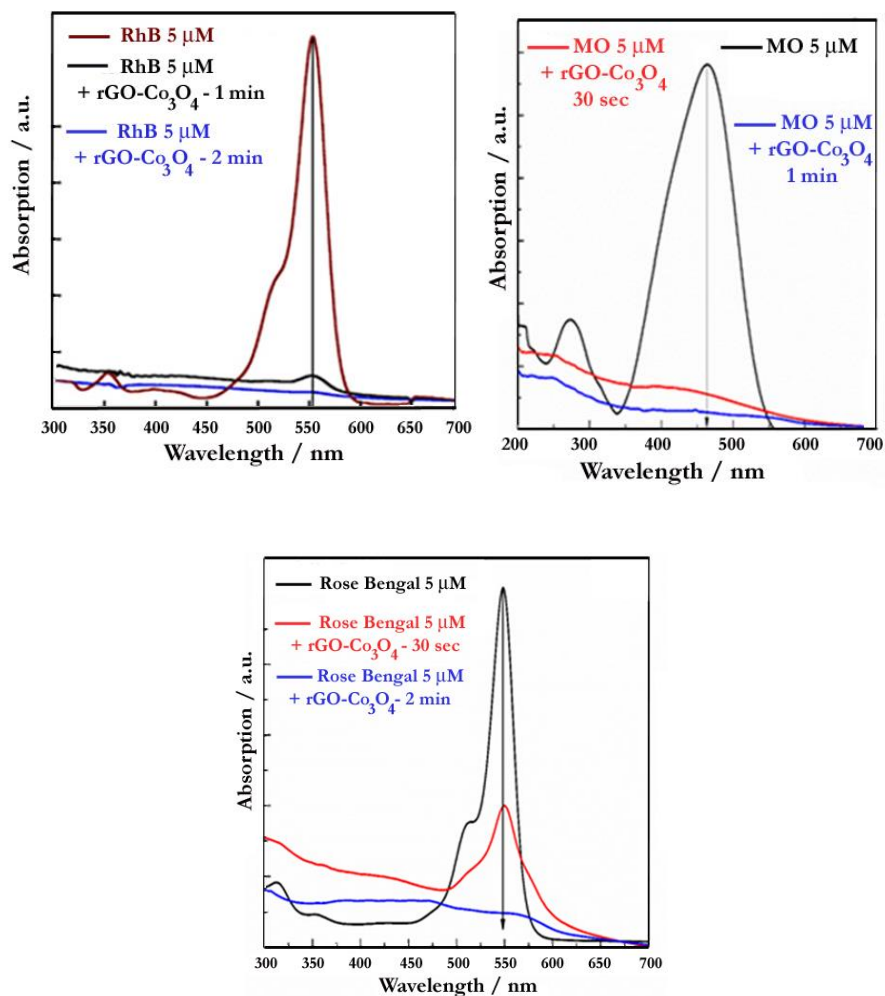


Figure 11: UV-Vis spectra of the a) RhB, b) MO, c) Rose Bengal solutions before and after adsorbent treatment. The initial concentration of dyes is 5 μM , of $\text{rGO-Co}_3\text{O}_4$: 1 mg/mL , $T=25^\circ\text{C}$).

The concentration of the remaining dye was monitored by measuring the absorbance of solutions at 554 nm (RhB), 463 nm (MO) and 550 nm (RB), respectively (**Fig. 11, S8, S9**). The results indicate that $\text{rGO-Co}_3\text{O}_4$ nanocomposite is very efficient for dye adsorption with complete removal within 2, 1 and 2 min for RhB, MO and RB, respectively. The performance of the $\text{rGO-Co}_3\text{O}_4$ nanocomposite is quite high as compared to other graphene-based adsorbents (**Table S1**) with the benefit of being easily separated by applying an external magnet.

Fig. 12 displays photos of the adsorption process; the formation of transparent solutions upon application of an external magnet (1 Tesla) clearly indicates that the dyes have been successfully adsorbed by rGO-Co₃O₄ nanocomposite.



Figure 12: Photographs of (A) RhB, (B) MO and (C) Rose Bengal aqueous solutions (5 μM) before and after treatment with 1 mg/ml of rGO-Co₃O₄ nanocomposite. External magnet of 1 Tesla.

3.2.4. Removal by rGO: adsorption mechanism

To gain a better understanding on the important parameters that govern the adsorption process, we have applied rGO as adsorbent of RhB, MO and RB from aqueous solution (**Fig. 13**). Although rGO was efficient for dye removal, the adsorption process was quite longer than with rGO-Co₃O₄ nanocomposite; it took 20 min to remove 92% of RhB and 6 min to remove 75 % of MO. Surprisingly, rGO was not efficient for RB adsorption with only 8% removal after 50 min. Interestingly, under otherwise identical experimental conditions, rGO-Co₃O₄ nanocomposite removed 96%, 91% and 92% of RhB, MO and RB after 2, 1 and 2 min, respectively. From these results, we can conclude that hybridization of rGO with Co₃O₄ NPs has improved significantly its adsorption capacity for the three investigated dyes with the big advantage that they can be easily separated by an external magnet.

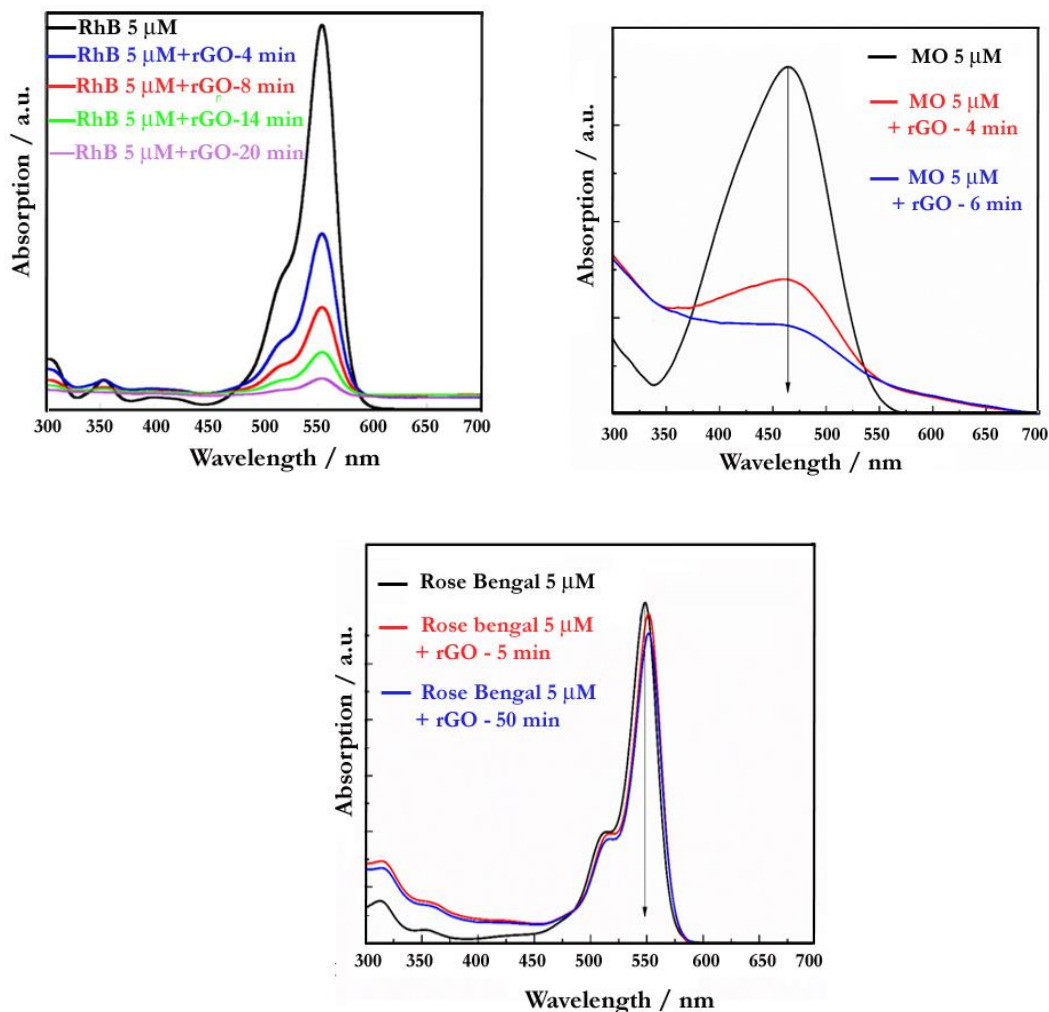


Figure 13: UV-Vis spectra of the original RhB, MO and Rose Bengal aqueous solutions before and after adsorbent treatment (initial concentration of dyes: 5 μM , rGO: 1 mg/mL, $T=25^\circ\text{C}$).

The mechanism of dye adsorption is controlled by various parameters such as the physical and/or chemical properties of the adsorbent. rGO nanosheets are capable of interacting with a dye molecule through π - π conjugation, H-bonding, electrostatic and hydrophobic interactions [38, 39]. Moreover, dye adsorption is strongly influenced by the surface area and surface functionality of adsorbents [3]. The surface structure of graphene has a strong influence on its adsorption capability. The surface of rGO- Co_3O_4 is positively charged under our experimental conditions (zeta potential of 17 ± 1.5 mV in water, **Fig. S6**). This implies that, for anionic dyes,

electrostatic interactions play a major role even though aromatic interactions (π - π stacking) are well recognized in adsorption processes of aromatic molecules on graphene surface. Moreover, the homogeneous dispersion of Co_3O_4 NPs over the rGO support results in enhanced surface area and improved adsorption ability. For cationic dyes, the interaction between the nanocomposite and the dyes is believed to be governed by π - π interactions rather than binding at the oxygen groups of the nanocomposite [40].

Our results prove that rGO- Co_3O_4 nanocomposite is an excellent, very efficient and fast dye adsorbent which works at neutral pH. Moreover, the rGO- Co_3O_4 hybrid is superparamagnetic at room temperature. Therefore, it can be easily and rapidly recovered from the solution through magnetic separation.

Conclusion

We have demonstrated that superparamagnetic rGO- Co_3O_4 nanocomposite exhibited good catalytic properties for 4-nitrophenol reduction to 4-aminophenol by NaBH_4 with a full reduction in less than 1 min. The nanocomposite can be reused for 10 consecutive catalytic cycles without any apparent loss of its activity, indicating a good stability. Furthermore, the nanocomposite displayed high adsorption capacity for Cr(VI) at room temperature. The adsorption process can be well described by the Langmuir model, suggesting monolayer coverage sorption of Cr(VI) on the surface of rGO- Co_3O_4 . The adsorption process of rGO- Co_3O_4 for Cr(VI) ions is pH dependent, reaching a higher adsorption capacity at low pH values. Finally, the nanocomposite was successfully applied for rhodamine B, methyl orange and rose Bengal (5-15 μM) removal in less than 1 min at neutral pH. More importantly, the magnetic properties of the nanocomposite permit its simple separation from the liquid phase by application of an external magnet (1 T). These results evidence that rGO- Co_3O_4 holds promise for potential applications for the removal of heavy metal ions and organic dyes from

wastewater, but also for other catalytic transformations in the field of environmental remediation.

Acknowledgements

The authors gratefully acknowledge financial support from the Centre National de la Recherche Scientifique (CNRS), the University Lille 1, and the Hauts-de-France region. The SEM facilities in Lille (France) are supported by the Conseil Régional des Hauts-De-France, the European Regional Development Fund (ERDF) and the CNRS.

References

- [1] C. Santhosh, V. Velmurugan, G. Jacob, S. K. Jeong, A. N. Grace, A. Bhatnagar, Role of nanomaterials in water treatment applications: A review, *Chem. Eng. J.*, 306 (2016) 1116-1137.
- [2] F. Depault, M. Cojocar, F. Fortin, S. Chakrabarti, N. Lemieux, Genotoxic effects of chromium(VI) and cadmium(II) in human blood lymphocytes using the electron microscopy in situ end-labeling (EM-ISEL) assay, *Toxicol. in Vitro*, 20 (2006) 513-518.
- [3] S. Wang, H. Sun, H. M. Ang, M. O. Tadé, Adsorptive remediation of environmental pollutants using novel graphene-based nanomaterials, *Chem. Eng. J.*, 226 (2013) 336-347.
- [4] L. Ren, H. Lu, L. Hea, Y. Zhang, Enhanced electrokinetic technologies with oxidation–reduction for organically-contaminated soil remediation, *Chem. Eng. J.*, 247 (2014) 111-124.
- [5] N. Ezzatahmedi, G. A. Ayoko, G. J. Millar, R. Speight, C. Yan, J. Li, S. Li, J. Zhu, Y. Xi, Clay-supported nanoscale zero-valent iron composite materials for the remediation of contaminated aqueous solutions: A review, *Chem. Eng. J.*, 312 (2017) 336-350.
- [6] J. Gómez-Pastora, E. Bringas, I. Ortiz, Recent progress and future challenges on the use of high performance magnetic nano-adsorbents in environmental applications, *Chem. Eng. J.*, 256 (2014) 187-204.

- [7] H. Wang, X. Yuan, Y. Wu, X. Chen, L. Leng, H. Wang, H. Li, G. Zeng, Facile synthesis of polypyrrole decorated reduced graphene oxide-Fe₃O₄ magnetic composites and its application for the Cr(VI) removal, *Chem. Eng. J.*, 262 (2015) 597-606.
- [8] H. C. Vu, A. D. Dwivedi, T. T. Le, S.-H. Seo, E.-J. Kim, Y.-S. Chang, Magnetite graphene oxide encapsulated in alginate beads for enhanced adsorption of Cr(VI) and As(V) from aqueous solutions: Role of crosslinking metal cations in pH control, *Chem. Eng. J.*, 307 (2017) 220-229.
- [9] L. Bai, Z. Li, Y. Zhang, T. Wang, R. Lu, W. Zhou, H. Gao, S. Zhang, Synthesis of water-dispersible graphene-modified magnetic polypyrrole nanocomposite and its ability to efficiently adsorb methylene blue from aqueous solution, *Chem. Eng. J.*, 279 (2015) 757-766.
- [10] Y. Ikedo, J. Sugiyama, H. Nozaki, H. Itahara, J. Brewer, E. Ansaldo, G. Morris, D. Andreica, A. Amato, Spatial inhomogeneity of magnetic moments in the cobalt oxide spinel Co₃O₄, *Phys. Rev. B*, 75 (2007) 054424.
- [11] Y. H. Li, K. L. Huang, D. M. Zeng, S. Q. Liu, Preparation and application of Co₃O₄ nanostructures with various morphologies, *Prog. Chem.*, 22 (2010) 2119-2125.
- [12] X. H. Xia, D. L. Chao, Y. Q. Zhang, Z. X. Shen, H. J. Fan, Three-dimensional graphene and their integrated electrodes, *nanotoday*, 9 (2014) 785-807.
- [13] P. Shi, R. Su, F. Wan, M. Zhu, D. Li, S. Xu, Co₃O₄ nanocrystals on graphene oxide as a synergistic catalyst for degradation of Orange II in water by advanced oxidation technology based on sulfate radicals, *Appl. Catal. B*, 123 (2012) 265-272.
- [14] C. X. Wang, P. H. Shi, X. D. Cai, Q. J. Xu, X. J. Zhou, X. L. Zhou, D. Yang, J. C. Fan, Y. L. Min, H. H. Ge, W. F. Yao, Synergistic effect of Co₃O₄ nanoparticles and graphene as catalysts for peroxymonosulfate-based Orange II degradation with high oxidant utilization efficiency, *J. Phys. Chem. C*, 120 (2016) 336-344.

- [15] P. H. Shi, R. J. Su, S. B. Zhu, M. C. Zhu, D. X. Li, S. H. Xu, Supported cobalt oxide on graphene oxide: Highly efficient catalysts for the removal of Orange II from water, *J. Hazard. Mater.*, 229 (2012) 331-339.
- [16] P. Shi, X. Dai, H. Zheng, D. Li, W. Yao, C. Hu, Synergistic catalysis of Co_3O_4 and graphene oxide on $\text{Co}_3\text{O}_4/\text{GO}$ catalysts for degradation of Orange II in water by advanced oxidation technology based on sulfate radicals, *Chem. Eng. J.*, 240 (2014) 264-270.
- [17] Y. J. Yao, Z. H. Yang, H. Q. Sun, S. B. Wang, Hydrothermal synthesis of Co_3O_4 -graphene for heterogeneous activation of peroxymonosulfate for decomposition of phenol, *Ind. Eng. Chem. Res.*, 51 (2012) 14958-14965.
- [18] E. Yavuz, S. Tokalioglu, H. Sxahan, S. Patat, A graphene/ Co_3O_4 nanocomposite as a new adsorbent for solid phase extraction of Pb(II), Cu(II) and Fe(III) ions in various samples, *RSC Adv.*, 3 (2013) 24650-24657.
- [19] O. Fellahi, M. R. Das, Y. Coffinier, S. Szunerits, T. Hadjersi, M. Maamache, R. Boukherroub, Silicon nanowire arrays-induced graphene oxide reduction under UV irradiation, *Nanoscale*, 3 (2011) 4662-4669.
- [20] V. Panwar, A. Al-Nafiey, A. Addad, B. Sieber, P. Roussel, R. Boukherroub, S. L. Jain, Magnetic Co_3O_4 /reduced graphene oxide nanocomposite as a superior heterogeneous catalyst for one-pot oxidative esterification of aldehydes to methyl esters, *RSC Adv.*, 5 (2015) 88567–88573.
- [21] S. Farhadi, K. Pourzare, S. Sadeghinejad, Simple preparation of ferromagnetic Co_3O_4 nanoparticles by thermal dissociation of the $[\text{CoII}(\text{NH}_3)_6](\text{NO}_3)_2$ complex at low temperature, *J. Nanostructure Chem.*, 3 (2013) 16.
- [22] N. Zhang, J. Shi, S. S. Mao, L. Guo, Co_3O_4 quantum dots: reverse micelle synthesis and visible-light-driven photocatalytic overall water splitting, *Chem. Commun.*, 50 (2014) 2002-2004.

- [23] S.-Q. Liu, B. Xiao, L.-R. Feng, S.-S. Zhou, Z.-G. Chen, C.-B. Liu, F. Chen, Z.-Y. Wu, N. Xu, W.-C. Oh, Z.-D. Meng, Graphene oxide enhances the Fenton-like photocatalytic activity of nickel ferrite for degradation of dyes under visible light irradiation, *Carbon*, 64 (2013) 197-206.
- [24] I. S. Hosu, Q. Wang, A. Vasilescu, S. F. Peteu, V. Raditoiu, S. Railian, V. Zaitsev, K. Turcheniuk, Q. Wang, M. Li, R. Boukherroub, S. Szunerits, Cobalt phthalocyanine tetracarboxylic acid modified reduced graphene oxide: a sensitive matrix for the electrocatalytic detection of peroxydinitrite and hydrogen peroxide, *RSC Adv.*, 5 (2015) 1474-1484.
- [25] Q. Wang, Q. Wang, M. Li, S. Szunerits, R. Boukherroub, One-step synthesis of Au nanoparticles-graphene composite using tyrosine: Electrocatalytic and catalytic properties, *New J. Chem.*, 40 (2016) 5473-5482.
- [26] D. Dinda, A. Gupta, S. K. Saha, Removal of toxic Cr(VI) by UV-active functionalized graphene oxide for water purification, *J. Mater. Chem. A*, 1 (2013) 11221-11228.
- [27] S. Li, X. Lu, Y. Xue, J. Lei, T. Zheng, C. Wang, Fabrication of polypyrrole/graphene oxide composite nanosheets and their applications for Cr(VI) removal in aqueous solution, *PloS One*, 7 (2012) e43328.
- [28] S. Zhang, M. Zeng, W. Xu, J. Li, J. Li, J. Xu, X. Wang, Polyaniline nanorods dotted on graphene oxide nanosheets as a novel super adsorbent for Cr (VI), *Dalton Trans.*, 42 (2013) 7854-7858.
- [29] M. Bhaumik, A. Maity, V. V. Srinivasu, M. S. Onyango, Enhanced removal of Cr(VI) from aqueous solution using polypyrrole/Fe₃O₄ magnetic nanocomposite, *J. Hazard. Mater.*, 190 (2011) 381-390.

- [30] K. Bhowmik, A. Mukherjee, M. Kr Mishra, G. De, Stable Ni Nanoparticle–Reduced Graphene Oxide Composites for the Reduction of Highly Toxic Aqueous Cr(VI) at Room Temperature, *Langmuir*, 30 (2014) 3209-3216.
- [31] J. H. Chen, H. T. Xing, H. X. Guo, W. Weng, S. R. Hu, S. X. Li, Y. H. Huang, X. Sun, Z. B. Su, Investigation on the adsorption properties of Cr(VI) ions on a novel graphene oxide (GO) based composite adsorbent, *J. Mater. Chem. A*, 2 (2014) 12561-12570.
- [32] L. Li, H. Duan, X. Wang, C. Luo, Adsorption property of Cr(VI) on magnetic mesoporous titanium dioxide–graphene oxide core–shell microspheres, *New J. Chem.*, 38 (2014) 6008-6016.
- [33] R. Dubey, J. Bajpai, A. K. Bajpai, Green synthesis of graphene sand composite (GSC) as novel adsorbent for efficient removal of Cr(VI) ions from aqueous solution, *J. Water Process Eng.*, 5 (2015) 83-94.
- [34] L. Fan, C. Luo, M. Sun, H. Qiu, Synthesis of graphene oxide decorated with magnetic cyclodextrin for fast chromium removal, *J. Mater. Chem.*, 22 (2012) 24577-24583.
- [35] L. Li, L. Fan, M. Sun, H. Qiu, X. Li, H. Duan, C. Luo, Adsorbent for chromium removal based on graphene oxide functionalized with magnetic cyclodextrin-chitosan, *Colloids Surf. B.: Biointerfaces*, 107 (2013) 76-83.
- [36] H. Jabeen, V. Chandra, S. Jung, J. W. Lee, K. S. Kim, S. B. Kim, Enhanced Cr(VI) removal using iron nanoparticle decorated graphene, *Nanoscale*, 3 (2011) 3583-3585.
- [37] S. Wang, W. Yang, G. Chen, Graphene-decorated porous ceramics for efficient removal of Cr(VI), *RSC Adv.*, 5 (2015,) 65982-65990.
- [38] T.-Y. Lin, D.-H. Chen, One-step green synthesis of arginine-capped iron oxide/reduced graphene oxide nanocomposite and its use for acid dye removal *RSC Adv.*, 4 (2014) 29357-29364.

[39] R. Gong, J. Ye, W. Dai, X. Yan, J. Hu, X. Hu, S. Li, H. Huang, Adsorptive removal of methyl orange and methylene blue from aqueous solution with finger-citron-residue-based activated carbon, *Ind. Eng. Chem. Res.*, 52 (2013) 14297-14303.

[40] Y. Qin, M. Long, B. Tan, B. Zhou, RhB Adsorption Performance of Magnetic Adsorbent Fe₃O₄/RGO Composite and Its Regeneration through A Fenton-like Reaction, *Nano-Micro Lett.*, 6 (2014) 125-135.